SUPPLEMENTARY INFORMATION

The hDIS3L2 exonuclease specifies a parallel 3'-5' degradation pathway of human cytoplasmic mRNA

Michal Lubas[1,2,3,4], Christian K. Damgaard[2], Rafal Tomecki [3,4], Dominik Cysewski[3,4], Torben Heick Jensen[1,2,*] and Andrzej Dziembowski[3,4*]

INDEX OF SUPPLEMENTARY INFORMATION

Supplemental figure legends

Figure S1. Multiple sequence alignment of RNase R, RNase II and Dis3 proteins. (A) RNAse R, RNase II, Dis3p, hDIS3, hDIS3L and hDIS3L2 were aligned using PROMALS3D (Materials and Methods). Evolutionarily conserved protein domains are indicated above the sequences. Amino acid residues are colored by percentage identity (blue gradient). The hDIS3L2 specific extension of the CSD1 domain is highlighted in yellow and the RNB active site is marked by a red frame.

(B) Phylogenetic analysis of hDIS3L2, hDIS3L, hDIS3 and their eukaryotic and prokaryotic homologs. Maximum likelihood tree was constructed based on RNB domain alignments. Dis3L2 proteins are widespread in eukaryotes and form a distant linage from the Dis3 family.

Figure S2. hDIS3L2 is a processive 3'-5' exonuclease active towards both ss- and ds-RNA.

(A) SDS-PAGE analysis of recombinant full-length wild-type hDIS3L2 protein ($hDIS3L2^{WT}$) and its variant bearing the D391N mutation within the RNB domain catalytic site ($hDIS3L2^{mut}$). PageRuler^{TM} Prestained Protein Ladder (Fermentas) with molecular masses indicated was used as a marker.

(B) Ion exchange chromatography of $hDIS3L2^{WT}$. Indicated fractions of $hDIS3L2^{WT}$ were incubated with a fluorescently labeled linear ss17-A_{34} RNA substrate (bottom of image). Fractions C3 and C4 were used for the analyses of hDIS3L2 biochemical properties. No activity of $hDIS3L2^{mut}$ towards RNA substrate was observed (data not shown).

(C) TLC analysis of the RNA degradation capabilities of hDIS3L2^{WT} and hDIS3L2^{mut} from (A). Single-stranded ss17-A_{14} oligoribonucleotide, 3'end-labeled with [^{32}P]pCp, was incubated with equal amounts of hDIS3L2^{WT}, hDIS3L2^{mut} or hDIS3^{WT} (positive control). Sample aliquots were collected at indicated time points and spotted onto a PEI-cellulose TLC plate, which was subsequently developed in the direction shown with the vertical arrow. Positions of substrate and product (pCp) are indicated. pCp-labeled RNAs are substrates of exoribonucleases from the RNAseR family, which accept the 3'phosphate (Vincent et al. 2006).

(D) hDIS3L2 activity is relatively insensitive to the concentration of magnesium or manganese ions, but is inhibited by elevated concentrations of zinc ions. The linear ss17-A_{14} RNA substrate was incubated with hDIS3L2^{WT} in various buffers, containing magnesium, manganese or zinc cations at different concentrations, as indicated. Reactions were terminated at the indicated time points followed by denaturing PAGE and phosphorimaging.

(E) hDIS3L2 displays 3'-5' exoribonuclease activity towards ssRNA. Wild-type hDIS3L2^{WT} or hDIS3L2^{mut} proteins were incubated in the presence of Mg^{2+} ions with 5'radiolabeled single-stranded 17nt RNA oligonucleotide substrates bearing adenosine extensions of different lengths (A_5 or A_{14}), as indicated. Control reactions were performed in the absence of added protein (no protein). Reactions were terminated at the indicated time points and the products were analyzed by 20% acrylamide/7M urea PAGE followed by phosphorimaging.

(F) Final reaction products of hDIS3L2 exoribonucleolytic degradation are shorter than those generated by the hDIS3 enzyme. Reactions were carried

out as in (E) using single-stranded ss17-A_{14} ssRNA substrate. Positions of 3–5 nt-long degradation products are marked with arrows.

(G) hDIS3L2 and hDIS3 display similar activities against ssRNA. $hDIS3^{WT}$, $hDIS3L2^{WT}$ or $hDIS3L2^{mut}$ proteins were incubated with single-stranded ss17-A_5 RNA oligonucleotide substrates as in (E), but the reactions were terminated at earlier time points, as indicated.

(H) hDIS3L2 is active towards dsRNA. RNase assays were performed as in (E), but using 5'radiolabeled partially structured double-stranded 17nt RNA substrates in which the longer (labeled) oligoribonucleotide possessed 3'ss oligoadenosine overhangs of different length (A_5 or A_{14}) as indicated.

(**I**) hDIS3L2 does not display endoribonucleolytic activity. A 5'-labelled and circularized ss17-A_{14} RNA substrate was incubated with $hDIS3L2^{WT}$ in various buffers containing magnesium, manganese or zinc cations and at different concentrations as indicated. Reaction products were analyzed as in (D).

(**J**) hDIS3L2 does not display 5'-3' exo- or endo-ribonucleolytic activity. RNase assays were conducted for 90 min using $hDIS3L2^{WT}$ or $hDIS3L2^{mut}$ in a buffer containing Mn^{2+} and 5'radiolabeled RNA substrate blocked at its 3'end by two deoxythymidine nucleotides to prevent 3'-5' exonucleolysis. Reaction products were analyzed as in (D).

Figure S3. Increased PB numbers upon hDIS3L2 depletion.

(A) Western blotting validation of hDIS3L2 and hXRN1 levels in EGFP (control), hDIS3L, hDIS3L2, hXRN1, hXRN1/hDIS3L and hXRN1/hDIS3L2 siRNA-treated HeLa cells used for PB analysis. Membranes were probed with the indicated antibodies. Actin was probed as a loading control.

(B) RT-qPCR validation of hDIS3L mRNA levels in EGFP (control), hDIS3L and hDIS3L/hXRN1 siRNA-treated HeLa cells used for PB analysis. PCR primers (Table S1) spanned an exon-exon junction of the hDIS3L mRNA. A U6-directed amplicon was used for normalization.

(C) Subcellular localization of hDCP1a (left) and hXRN1 (right) in HeLa cells treated with siRNAs against EGFP (control) or hDIS3L2. Proteins were visualized by fluorescence microscopy using 63X oil-immerse objective. Nuclei were stained with DAPI and merged with the localization of the respective proteins.

Figure S4. Validation of hDIS3L2, hXRN1 and hDIS3L depletions in HeLa cells used for RNA seq analysis.

(A) Western blotting validation of hDIS3L2 and hXRN1 protein levels in EGFP (control), hDIS3L, hDIS3L2, hXRN1, hXRN1/hDIS3L and hXRN1/hDIS3L2 siRNA-treated HeLa cells. Bars represent mean values of two biological replicates for each knockdown condition. Membranes were probed with the indicated antibodies. ImageJ was used for quantification.

(B) RNA-seq validation of hDIS3L mRNA levels in EGFP (control), hDIS3L, hDIS3L2, hXRN1, hXRN1/hDIS3L and hXRN1/hDIS3L2 siRNA-treated cells. Bars represent mean number of sequence reads in two biological replicates. The number of reads was normalized to the library size.

Figure S5. Correlation, quantification and verification of affected transcripts.

(A) Hierarchical clustering heatmap showing 200 differentially expressed

genes (DEGs) of the highest confidence (adjusted p-value with the Benjamin-Hochberg correction (padj)). The correlation dendrogram (top panel) indicates the relationship of gene-expression levels between the indicated conditions and replicates.

(B) Venn diagrams representing the quantity of indicated transcript groups and their overlap. Diagrams show all- (left), upregulated- (middle) (≥ 2-fold changed, padj ≤ 0.05) and downregulated- (right) (≤ 2-fold changed, padj ≤ 0.05) RNAs.

(C) DESeq scatter plots showing pair-wise comparisons of transcript levels between the indicated samples versus the control. Each dot represents the mean expression value of 2 replicates. DEGs are indicated in red.

(D) qRT-PCR validation of RNAseq data showing selected upregulated mRNAs from all single depletions. Each PCR reaction was performed in triplicate from two independent biological samples. Error bars calculated as standard error of the mean.

(E) qRT-PCR validation of selected mRNAs upregulated upon hDIS3L2 depletion using two different siRNAs (upper right: western blotting validation of depletions). qPCR data was normalized to levels of total RNA. Each PCR reaction was performed in triplicate and a representative experiment is shown. Western blotting analysis was performed as in S4A. The hDIS3L2#1 siRNA was used elsewhere in this study.

(F) Graphs representing highly enriched GO terms among non-redundant, upregulated mRNAs from hDIS3L2 (cellular component terms) and hXRN1 (biological and molecular function terms) knockdown samples clustered using DAVID. Only the most enriched clusters for each condition are shown.

Barplots represent percentage of GO terms within nonredundant upregulated mRNAs (-log(pvalue)).

Figure S1A

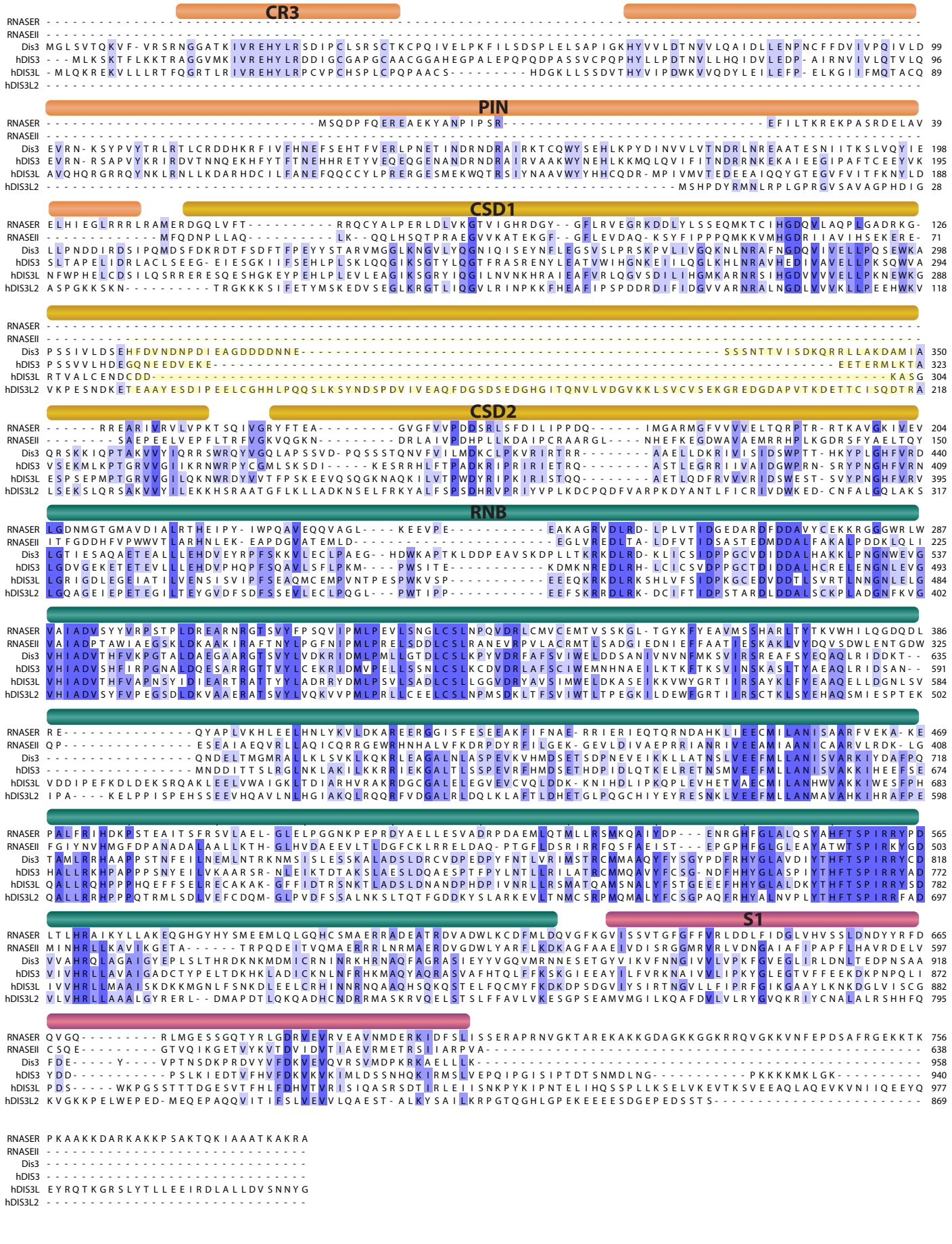
CR3
PIN
CSD1
CSD2
RNB
S1
RNASER
RNASEII
Dis3
hDIS3
hDIS3L
hDIS3L2

Figure S1B

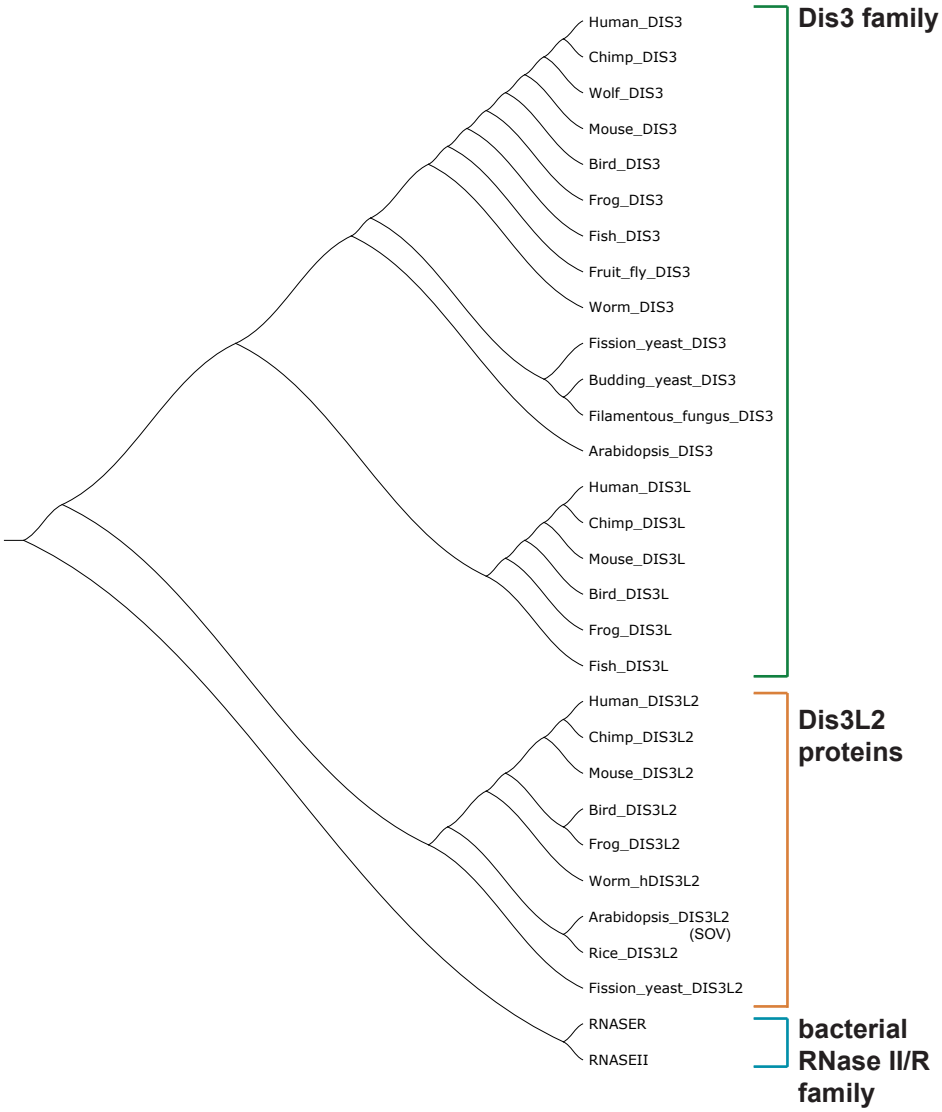
Human_DIS3
Chimp_DIS3
Wolf_DIS3
Mouse_DIS3
Bird_DIS3
Frog_DIS3
Fish_DIS3
Fruit_fly_DIS3
Worm_DIS3
Fission_yeast_DIS3
Budding_yeast_DIS3
Filamentous_fungus_DIS3
Arabidopsis_DIS3
Human_DIS3L
Chimp_DIS3L
Mouse_DIS3L
Bird_DIS3L
Frog_DIS3L
Fish_DIS3L
Human_DIS3L2
Chimp_DIS3L2
Mouse_DIS3L2
Bird_DIS3L2
Frog_DIS3L2
Worm_hDIS3L2
Arabidopsis_DIS3L2 (SOV)
Rice_DIS3L2
Fission_yeast_DIS3L2
RNASER
RNASEII
Dis3 family
Dis3L2 proteins
bacterial RNase II/R family

Figure S2

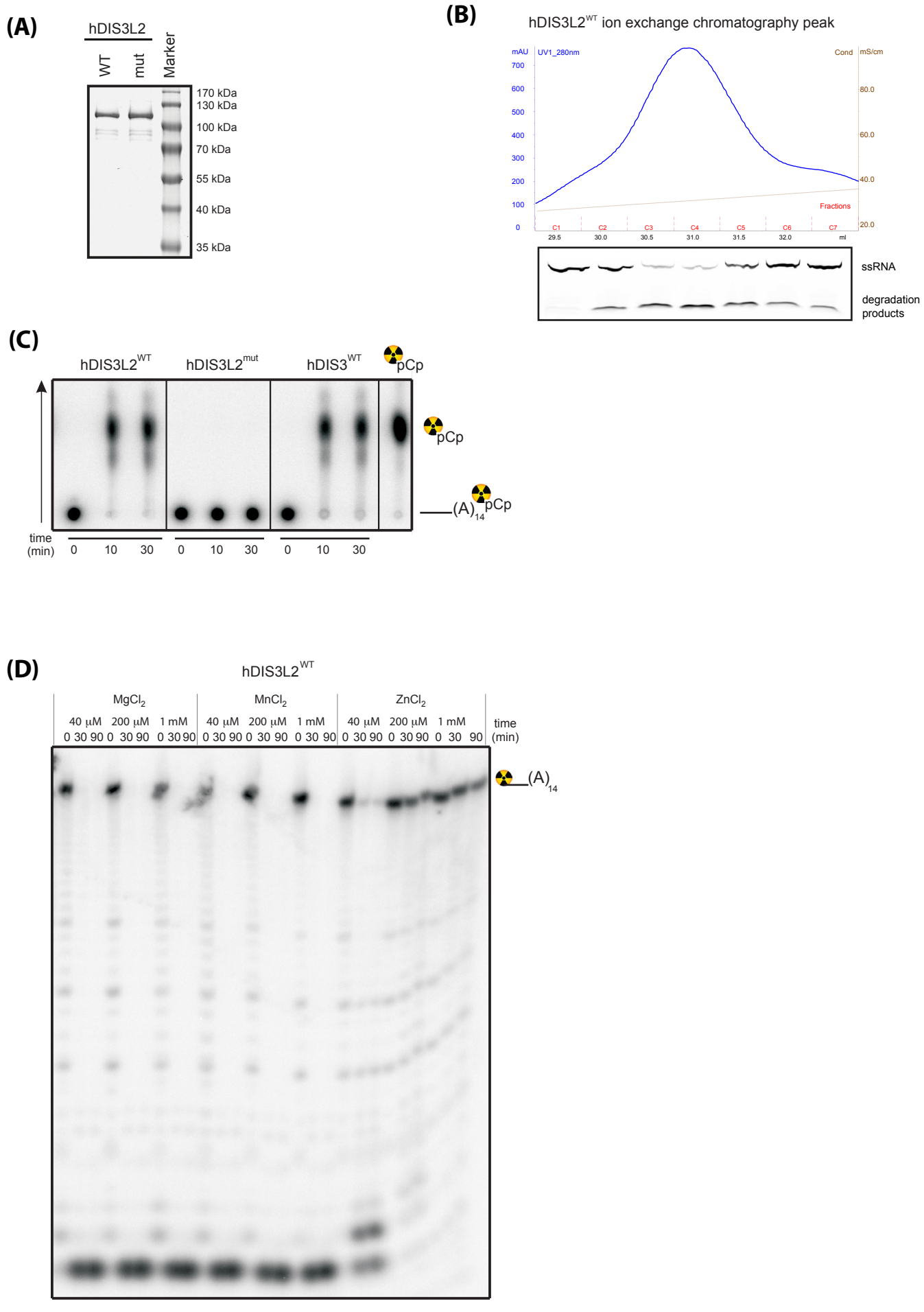
(A)
hDIS3L2
WT
mut
Marker
170 kDa
130 kDa
100 kDa
70 kDa
55 kDa
40 kDa
35 kDa
(B)
hDIS3L2WT ion exchange chromatography peak
mAU
UV1_280nm
Cond
mS/cm
Fractions
C1
C2
C3
C4
C5
C6
C7
ml
ssRNA
degradation products
(C)
hDIS3L2WT
hDIS3L2mut
hDIS3WT
pCp
(A)14pCp
time (min)
0
10
30
(D)
hDIS3L2WT
MgCl2
MnCl2
ZnCl2
40 µM
200 µM
1 mM
time (min)
(A)14

Figure S2

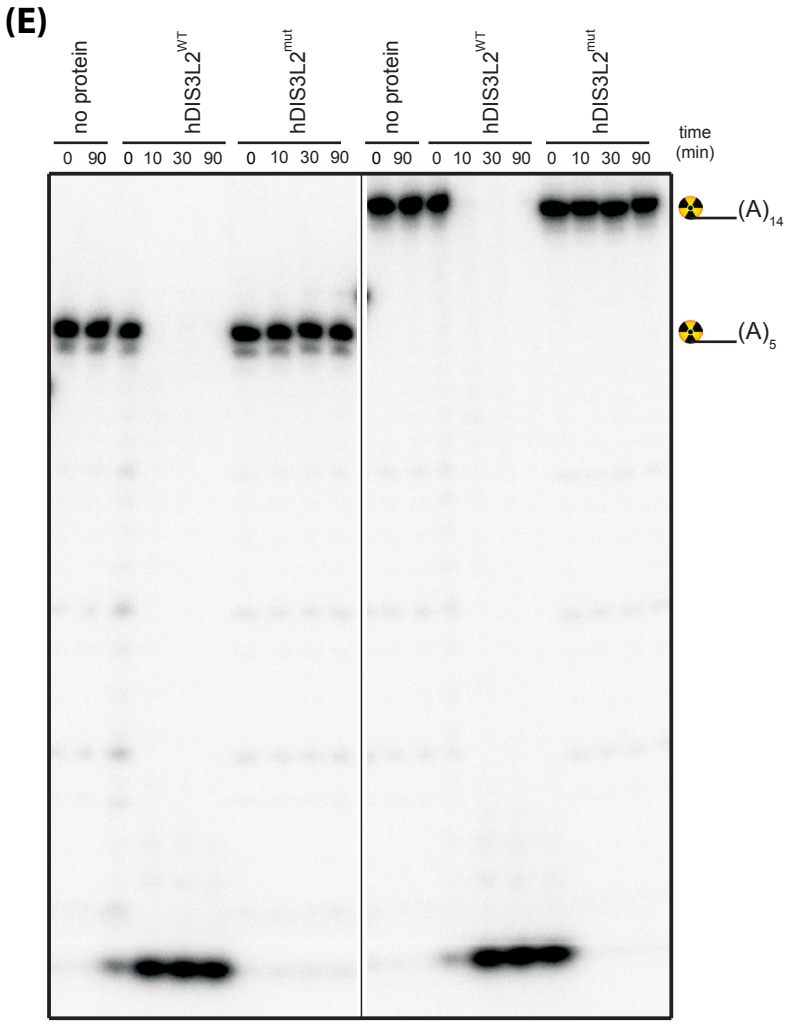
(E)
no protein
hDIS3L2WT
hDIS3L2mut
no protein
hDIS3L2WT
hDIS3L2mut
0 90 0 10 30 90 0 10 30 90 0 90 0 10 30 90 0 10 30 90
time (min)
(A)14
(A)5

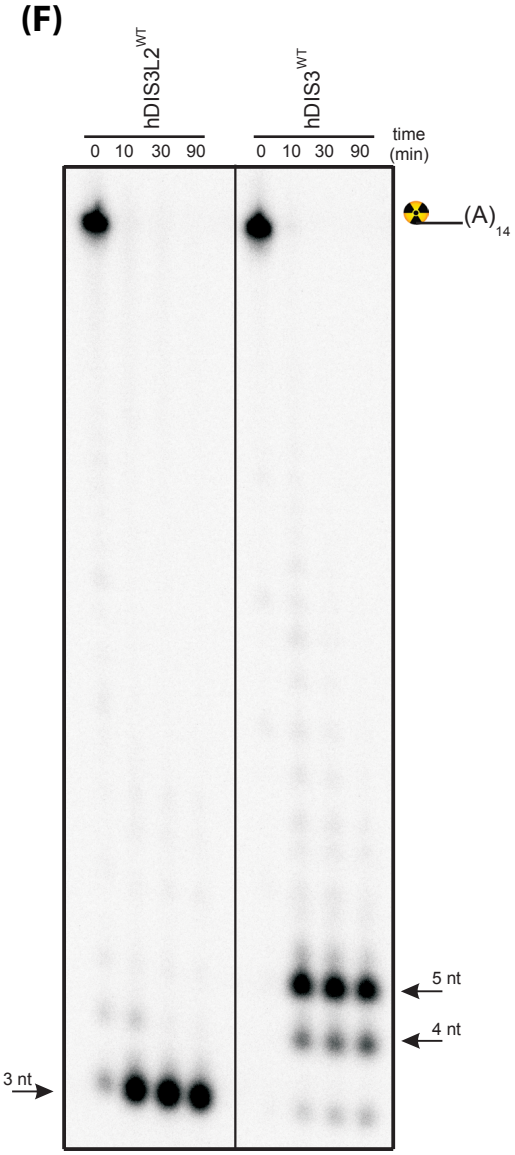
(F)
hDIS3L2WT
hDIS3WT
0 10 30 90 0 10 30 90
time (min)
(A)14
5 nt
4 nt
3 nt

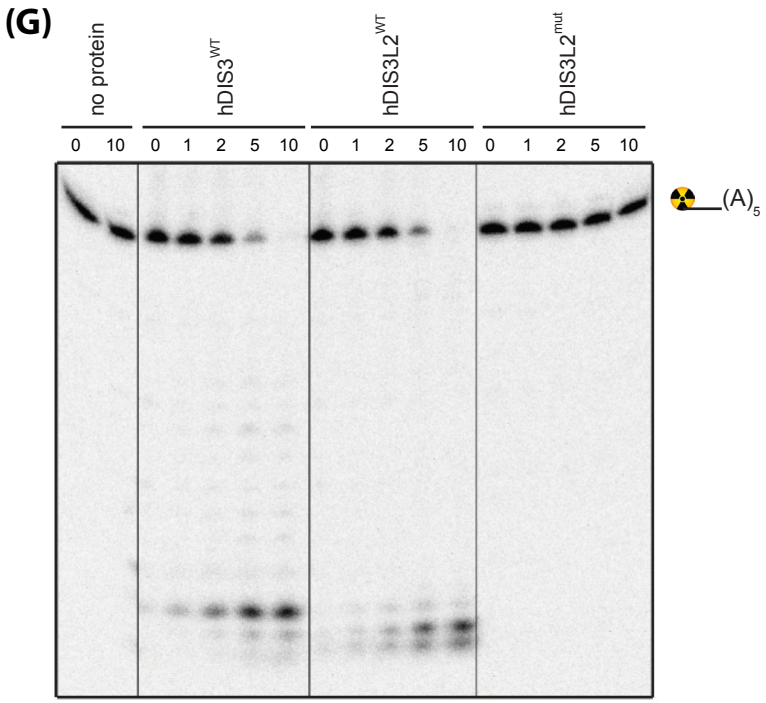
(G)
no protein
hDIS3WT
hDIS3L2WT
hDIS3L2mut
0 10 0 1 2 5 10 0 1 2 5 10 0 1 2 5 10
(A)5

Figure S2

(H)

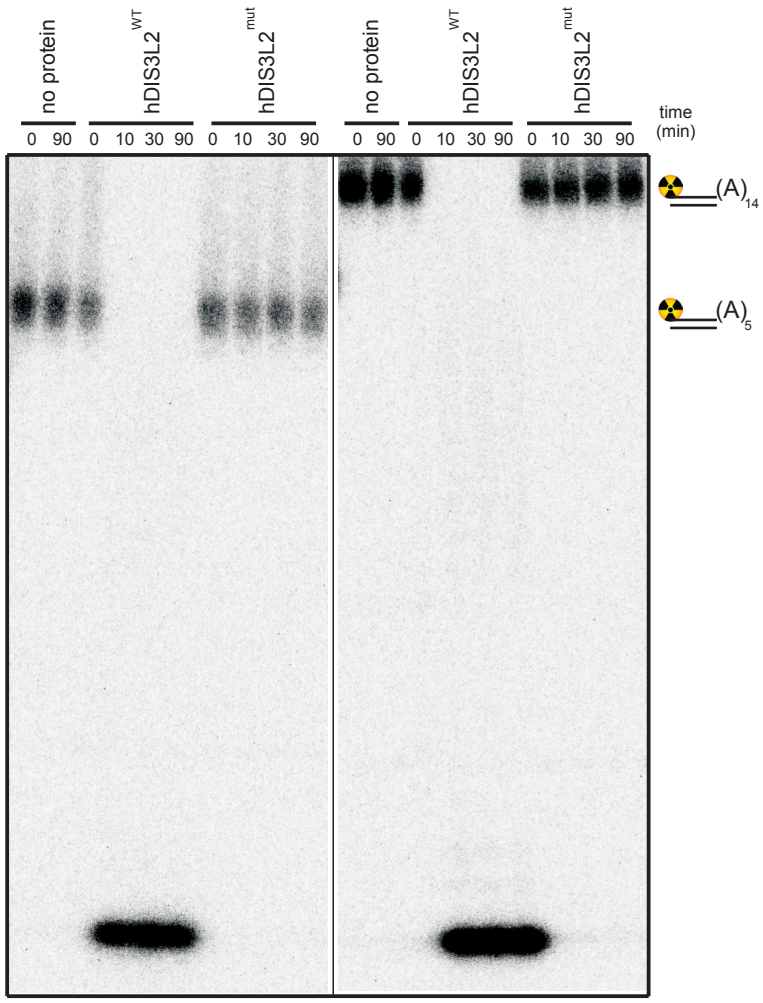

(I)

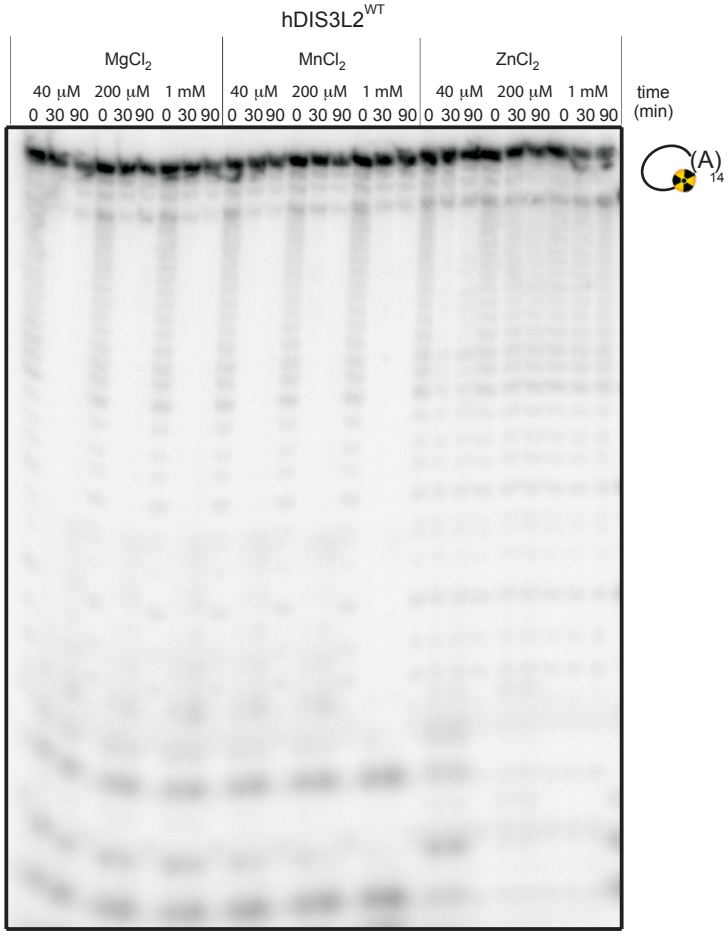

(J)

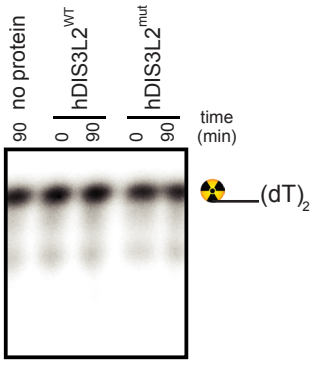

Figure S3

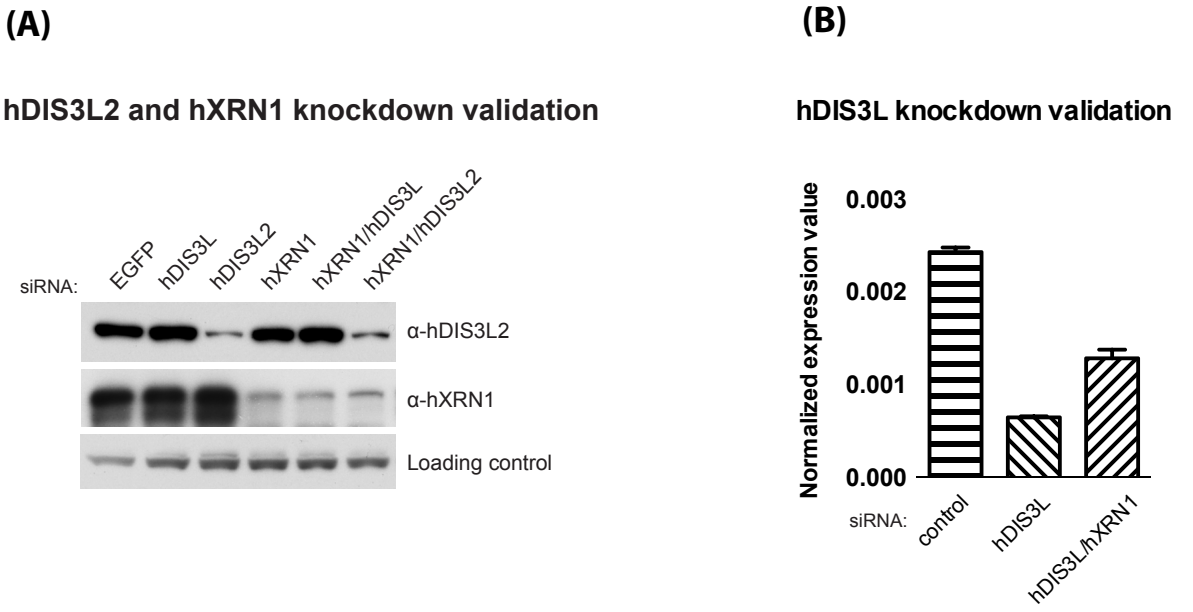
(A)
hDIS3L2 and hXRN1 knockdown validation
siRNA:
EGFP
hDIS3L
hDIS3L2
hXRN1
hXRN1/hDIS3L
hXRN1/hDIS3L2
α-hDIS3L2
α-hXRN1
Loading control
(B)
hDIS3L knockdown validation
Normalized expression value
0.003
0.002
0.001
0.000
siRNA:
control
hDIS3L
hDIS3L/hXRN1
(C)
siRNA
control
α-hDCP1a
merge
siRNA
control
α-hXRN1
merge
hDIS3L2
α-hDCP1a
merge
hDIS3L2
α-hXRN1
merge

Figure S4

(A)

hDIS3L2 and hXRN1 knockdown validation (average fold change western blotting analysis)

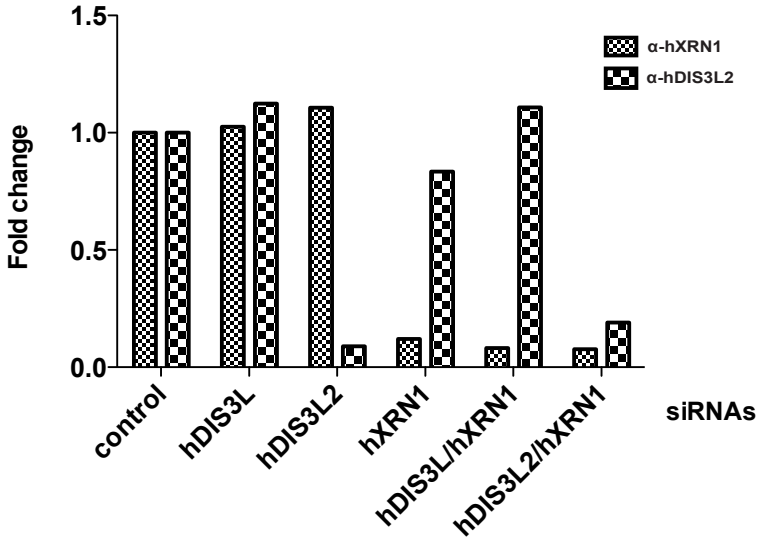

(B)

hDIS3L knockdown validation (average change in RNAseq libraries)

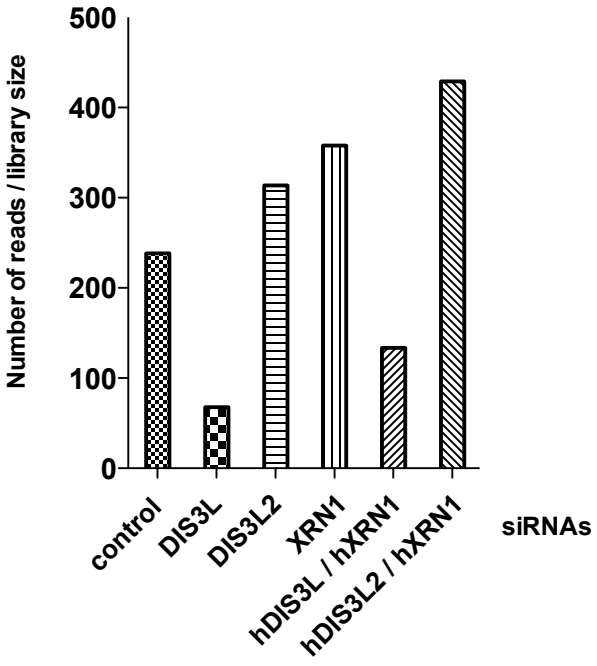

Figure S5

(A)

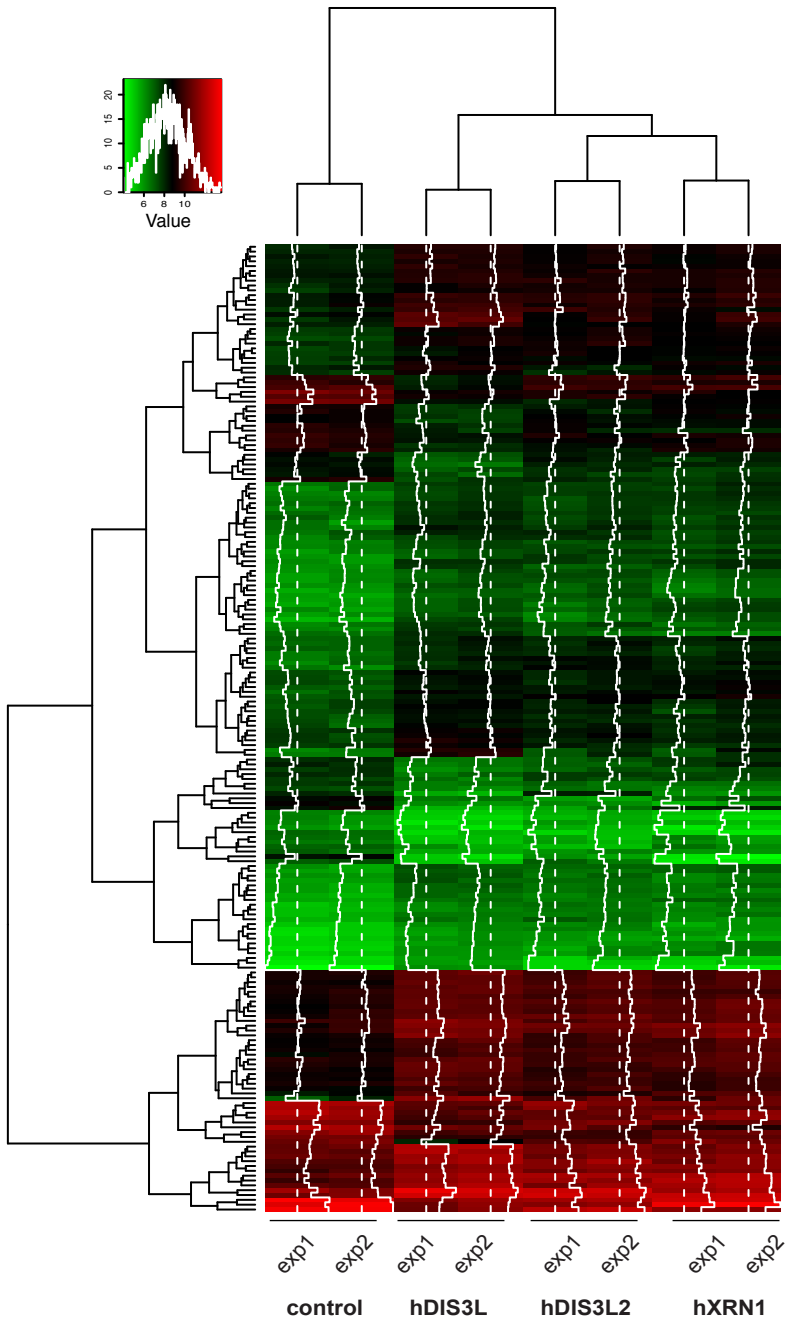
Hierarchical clustering heatmap
Value
exp1
exp2
exp1
exp2
exp1
exp2
exp1
exp2
control
hDIS3L
hDIS3L2
hXRN1

Figure S5

(B)

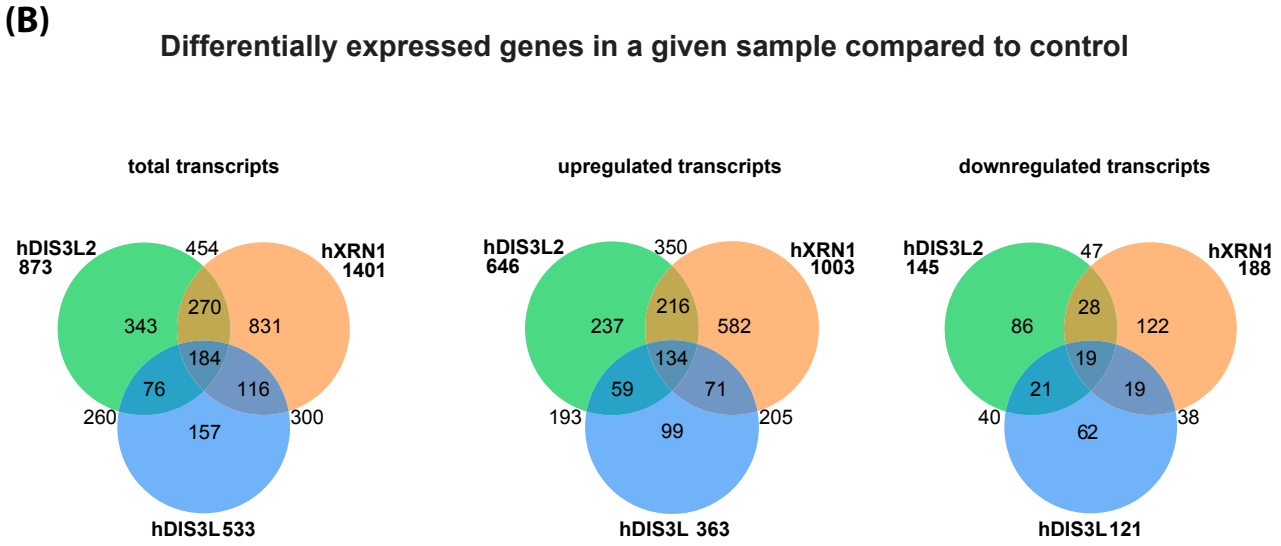
Differentially expressed genes in a given sample compared to control
total transcripts
hDIS3L2
873
454
hXRN1
1401
343
270
831
184
76
116
260
157
300
hDIS3L 533
upregulated transcripts
hDIS3L2
646
350
hXRN1
1003
237
216
582
134
59
71
193
99
205
hDIS3L 363
downregulated transcripts
hDIS3L2
145
47
hXRN1
188
86
28
122
19
21
19
40
62
38
hDIS3L 121

Figure S5

(C)

Pair-wise comparisons of gene expression of knockdowns versus control

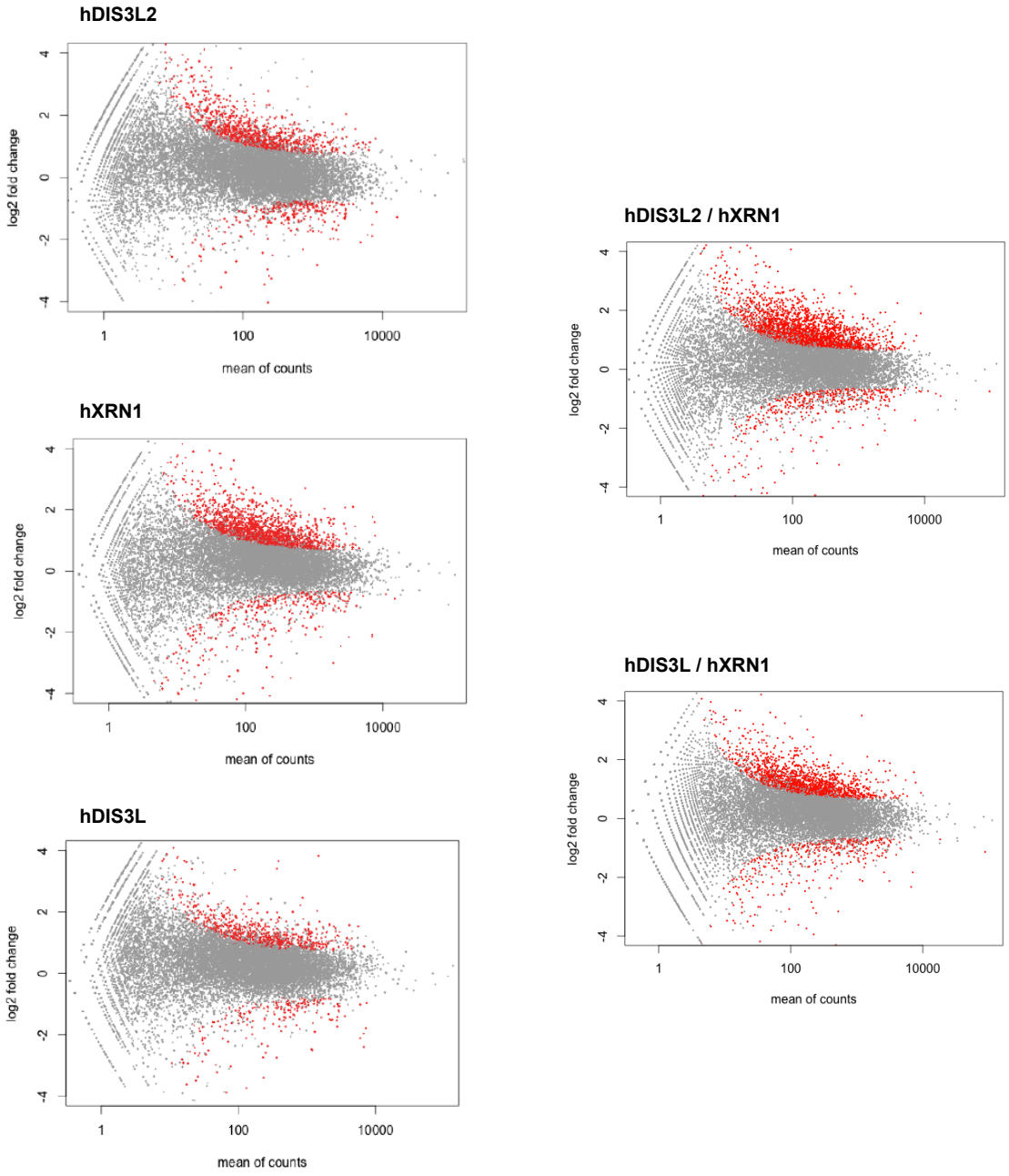

Figure S5

(D)

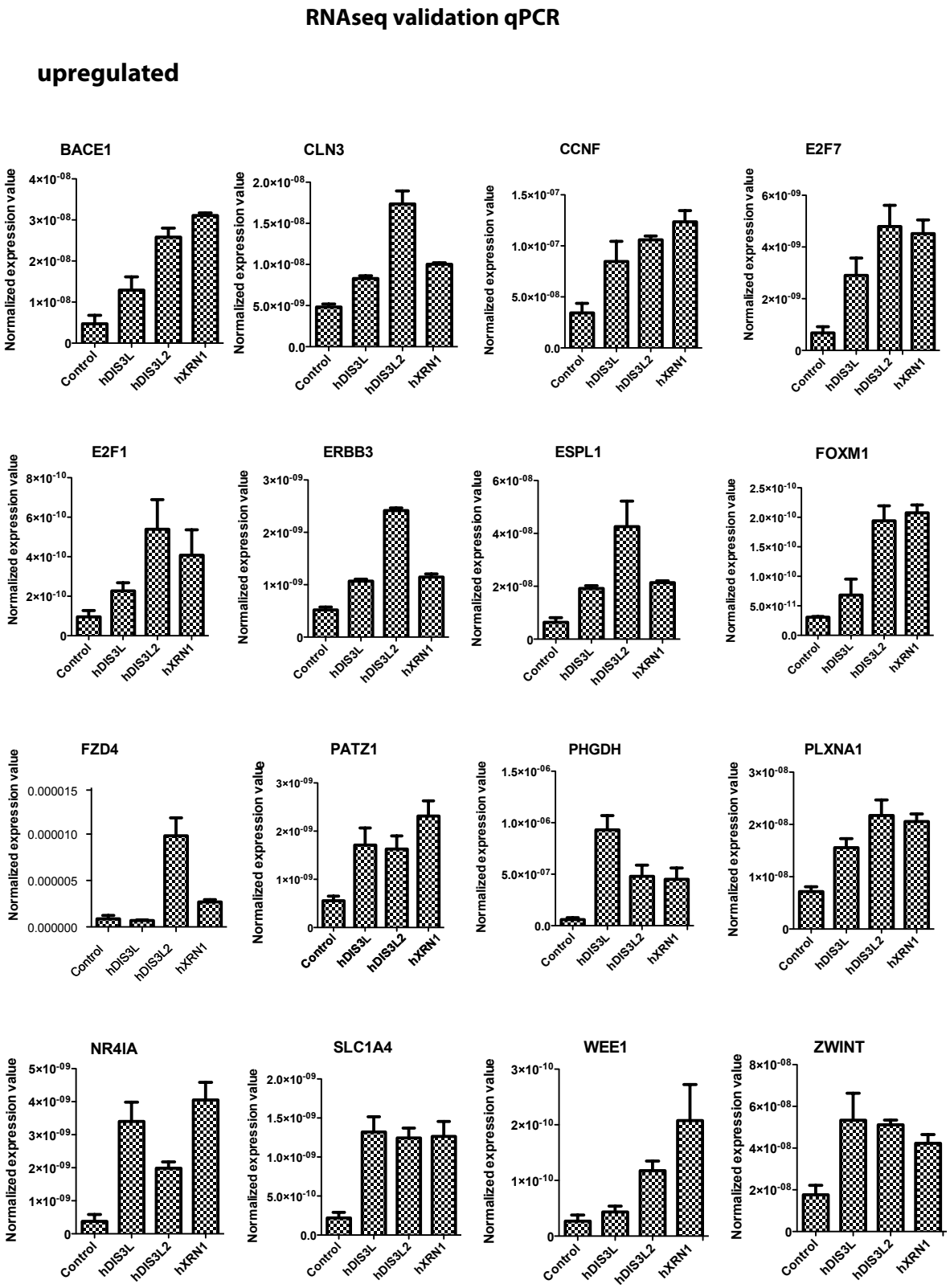
RNAseq validation qPCR
upregulated
BACE1
CLN3
CCNF
E2F7
E2F1
ERBB3
ESPL1
FOXM1
FZD4
PATZ1
PHGDH
PLXNA1
NR4IA
SLC1A4
WEE1
ZWINT
Normalized expression value
Control
hDIS3L
hDIS3L2
hXRN1

Figure S5

(E)

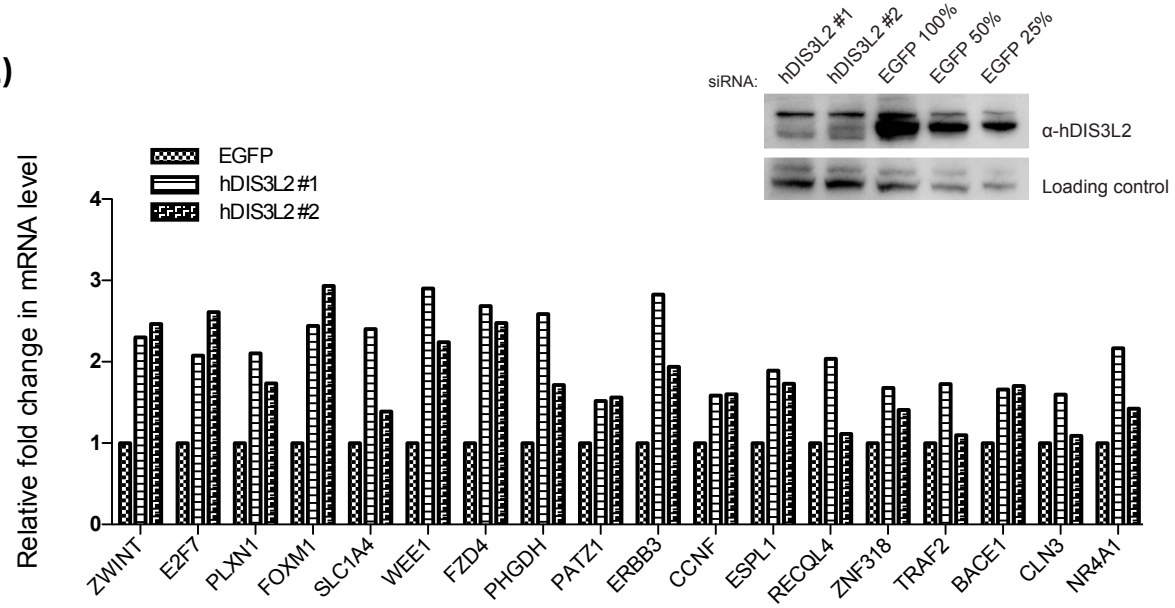
siRNA:
hDIS3L2 #1
hDIS3L2 #2
EGFP 100%
EGFP 50%
EGFP 25%
α-hDIS3L2
Loading control
EGFP
hDIS3L2 #1
hDIS3L2 #2
Relative fold change in mRNA level
0
1
2
3
4
ZWINT
E2F7
PLXN1
FOXM1
SLC1A4
WEE1
FZD4
PHGDH
PATZ1
ERBB3
CCNF
ESPL1
RECQL4
ZNF318
TRAF2
BACE1
CLN3
NR4A1

(F)

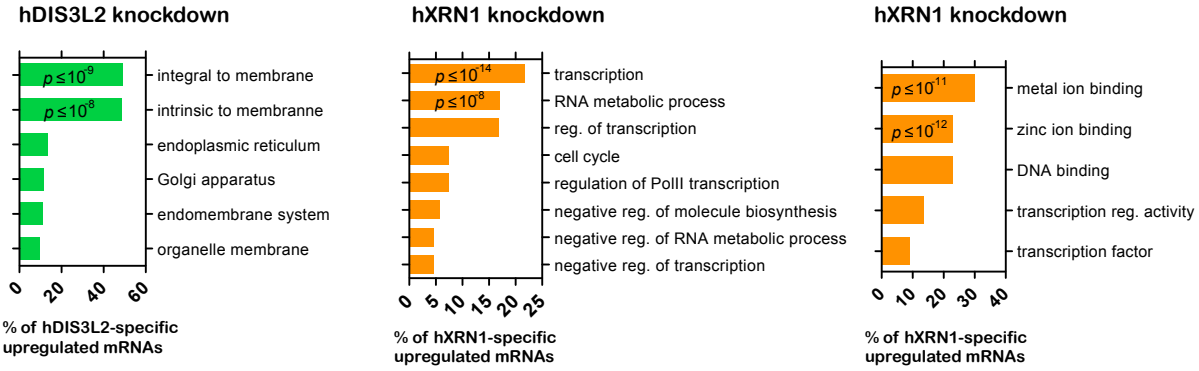
hDIS3L2 knockdown
p ≤10-9
p ≤10-8
integral to membrane
intrinsic to membranne
endoplasmic reticulum
Golgi apparatus
endomembrane system
organelle membrane
0
20
40
60
% of hDIS3L2-specific upregulated mRNAs
hXRN1 knockdown
p ≤10-14
p ≤10-8
transcription
RNA metabolic process
reg. of transcription
cell cycle
regulation of PolII transcription
negative reg. of molecule biosynthesis
negative reg. of RNA metabolic process
negative reg. of transcription
0
5
10
15
20
25
% of hXRN1-specific upregulated mRNAs
hXRN1 knockdown
p ≤10-11
p ≤10-12
metal ion binding
zinc ion binding
DNA binding
transcription reg. activity
transcription factor
0
10
20
30
40
% of hXRN1-specific upregulated mRNAs